Subwavelength topological structures resulting from surface two-plasmon resonance by femtosecond laser exposure solid surface

Hai-Ying Song,[1] **Shi-Bing Liu,**[1,*] **H. Y. Liu,**[2] **Yang Wang,**[1] **Tao Chen,**[1] **and Xiang-Ming Dong**[1]

[1]*Strong-field and Ultrafast Photonics Lab, Institute of Laser Engineering Beijing University of Technology, Beijing 100124, China*
[2]*Max-Planck Institute for the Structure and Dynamics of Matter, Hamburg, Germany*
[*]*sbliu@bjut.edu.cn*

Abstract: We present that surface two-plasmon resonance (STPR) in electron plasma sheet produced by a femtosecond laser irradiating a solid surface is the self-formation mechanism of periodic subwavelength ripple structures. Peaks of overdense electrons, formed by resonant two-plasmon wave mode, pull bound ions out of the metal surface. Thus, the wave pattern of STPR is "carved" on the surface by Coulomb ablation (removal) due to periodic distributed strong electrostatic field produced by charge separation. To confirm the STPR model, we have performed analogical carving experiments by two femtosecond laser beams with perpendicular polarizations and time delay. The results explicitly show that two wave patterns of STPR generated by each beam are independently created in the pulse exposure area of a target surface, which is like the traditional "layer-carving" technique by comparison with the structured topological features. The time-scale of ablation dynamics and the electron temperature in ultrafast interaction are also verified by a time-resolved spectroscopy experiment and numerical simulation, respectively. The present model can self-consistently explain the formation of subwavelength ripple structures even with spatial periods shorter than half of the laser wavelength, shedding light on the understanding of ultrafast laser-solid interaction.

OCIS codes: (350.3390) Laser materials processing; (260.7120) Ultrafast phenomena; (310.6628) Subwavelength structures.

References and links

1. J. E. Sipe, J. F. Young, J. S. Preston, and H. M. van Driel, "Laser-induced periodic surface structure. I. Theory," Phys. Rev. B **27**(2), 1141–1154 (1983).
2. A. Borowiec and H. K. Haugen, "Subwavelength ripple formation on the surfaces of compound semiconductors irradiated with femtosecond laser pulses," Appl. Phys. Lett. **82**(25), 4462–4464 (2003).
3. J. Bonse, M. Munz, and H. Sturm, "Structure formation on the surface of indium phosphide irradiated by femtosecond laser pulses," J. Appl. Phys. **97**(1), 013538 (2005).
4. J. Wang and C. Guo, "Formation of extraordinarily uniform periodic structures on metals induced by femtosecond laser pulses," J. Appl. Phys. **100**(2), 023511 (2006).
5. G. Miyaji and K. Miyazaki, "Origin of periodicity in nanostructuring on thin film surfaces ablated with femtosecond laser pulses," Opt. Express **16**(20), 16265–16271 (2008).

#255940 Received 18 Dec 2015; revised 19 May 2016; accepted 20 May 2016; published 26 May 2016

6. M. Huang, F. Zhao, Y. Cheng, N. Xu, and Z. Xu, "Origin of laser-induced near-subwavelength ripples: interference between surface plasmons and incident laser," ACS Nano **3**(12), 4062–4070 (2009).
7. J. Bonse, A. Rosenfeld, and J. Krüger,"On the role of surface plasmon polaritons in the formation of laser-induced periodic surface structures upon irradiation of silicon by femtosecond-laser pulses," J. Appl. Phys. **106**(10), 104910 (2009).
8. F. Garrelie, J. P. Colombier, F. Pigeon, S. Tonchev, N. Faure, M. Bounhalli, S. Reynaud, and O. Parriaux, "Evidence of surface plasmon resonance in ultrafast laser-induced ripples," Opt. Express **19**(10), 9035–9043 (2011).
9. D. C. Emmony, R. P. Howson, and L. J. Willis, "Laser mirror damage in germanium at 10.6 μm," Appl. Phys. Lett. **23**(11), 598–600 (1973).
10. G. Zhou, P. M. Fauchet, and A. E. Siegman, "Growth of spontaneous periodic surface structures on solids during laser illumination," Phys. Rev. B **26**(10), 5366–5381 (1982).
11. J. F. Young, J. S. Preston, H. M. van Driel, and J. E. Sipe, "Laser-induced periodic surface structure.II. Experiments on Ge, Si, Al, and brass," Phys. Rev. B **27**(2), 1155–1172 (1983).
12. S. Sakabe, M. Hashida, S. Tokita, S. Namba, and K. Okamuro, "Mechanism for self-formation of periodic grating structures on a metal surface by a femtosecond laser pulse," Phys. Rev. B **79**(3), 033409 (2009).
13. K. Okamuro, M. Hashida, Y. Miyasaka, Y. Ikuta, S. Tokita, and S. Sakabe, "Laser fluence dependence of periodic grating structures formed on metal surfaces under femtosecond laser pulse irradiation," Phys. Rev. B **82**(16), 165417 (2010).
14. L. Gemini, M. Hashida, M. Shimizu, Y. Miyasaka, S. Inoue, S. Tokita, J. Limpouch, T. Mocek, and S. Sakabe, "Metal-like self-organization of periodic nanostructures on silicon and silicon carbide under femtosecond laser pulses," J. Appl. Phys. **114**(19), 194903 (2013).
15. J. Reif, F. Costache, M. Henyk, and S. V. Pandelov, "Ripples revisited: non-classical morphology at the bottom of femtosecond laser ablation craters in transparent dielectrics," Appl. Surf. Sci. **197–198**, 891–895 (2002).
16. M. Henyk, N. Vogel, D. Wolfframm, A. Tempel, and J. Reif, "Femtosecond laser ablation from dielectric materials: Comparison to arc discharge erosion," Appl. Phys. A **69**, S355–S358 (1999).
17. A. Y. Vorobyev and C. Guo, "Direct femtosecond laser surface nano/microstructuring and its applications," Laser Photonics Rev. **7**(3), 385–407 (2013).
18. M. Straub, M. Afshar, D. Feili, H. Seidel, and K. König, "Surface plasmon polariton model of high-spatial frequency laser-induced periodic surface structure generation in silicon," J. Appl. Phys. **111**(12), 124315 (2012).
19. Y. Huang, S. Liu, W. Li, Y. Liu, and W. Yang, "Two-dimensional periodic structure induced by single-beam femtosecond laser pulses irradiating titanium," Opt. Express **17**(23), 20756–20761 (2009).
20. J. Bonse, J. Krüger, S. Höhm, and A. Rosenfeld, "Femtosecond laser-induced periodic surface structures," J. Laser Appl. **24**(4), 042006 (2012).
21. K. M. T. Ahmmed, C. Grambow, and A. Kietzig, "Fabrication of micro/nano structures on metals by femtosecond laser micromachining," Micromachines **5**, 1219–1253 (2014).
22. L. V. Keldysh, "Ionization in the field of a strong electromagnetic wave," Sov. Phys. JETP **20**(5), 1307–1314 (1965).
23. M. Tsukamoto, K. Asuka, H. Nakano, M. Hashida, M.Katto, N. Abe, and M. Fujita, "Periodic microstructures produced by femtosecond laser irradiation on titanium plate," Vacuum. **80**, 1346–1350 (2006).
24. A. Y. Vorobyev and C. Guo, "Femtosecond laser structuring of titanium implants," Appl. Surf. Sci. **253**, 7272–7280 (2007).
25. V. Oliveira, S. Ausset, and R. Vilar, "Surface micro/nanostructuring of titanium under stationary and non-stationary femtosecond laser irradiation," Appl. Surf. Sci. **255**, 7556–7560 (2009).
26. A. Y. Vorobyev and C. Guo, "Colorizing metals with femtosecond laser pulses," Appl. Phys. Lett. **92**(4), 041914 (2008).
27. C. A. Zuhlke, T. P. Anderson, and D. R. Alexander, "Fundamentals of layered nanoparticle covered pyramidal structuresformed on nickel during femtosecond laser surface interactions," Appl. Surf. Sci. **283**, 648–653 (2013).
28. Q. Z. Zhao, S. Malzer, and L. J. Wang, "Formation of subwavelength periodic structures on tungsten induced by ultrashort laser pulses," Opt. Lett. **32**(13), 1932–1934 (2007).
29. A. Y. Vorobyev, V. S. Makin, and C. Guo, "Periodic ordering of random surface nanostructures induced by femtosecond laser pulses on metals," J. Appl. Phys. **101**(3), 034903 (2007).
30. J. W. Yao, C. Y. Zhang, H. Y. Liu, Q. F. Dai, L. J. Wu, S. Lan, A. V. Gopal, V. A. Trofimov, and T. M. Lysak, "High spatial frequency periodic structures induced on metal surface by femtosecond laser pulses," Opt. Express **20**(2), 905–911 (2012).
31. B. Wu, M. Zhou, J. Li, X. Ye, G. Li, and L. Cai, "Superhydrophobic surfaces fabricated by microstructuring of stainless steel using a femtosecond laser," Appl. Surf. Sci. **256**, 61–66 (2009).
32. P. Bizi-Bandoki, S. Benayoun, S. Valette, B. Beaugiraud, and E. Audouard, "Modifications of roughness and wettability properties of metals induced by femtosecond laser treatment," Appl. Surf. Sci. **257**, 5213–5218 (2011).
33. W. Rozmus and V. T. Tikhonchuk, "Skin effect and interaction of short laser pulses with dense plasmas," Phys. Rev. A **42**(12), 7401–7412 (1990).

#255940 Received 18 Dec 2015; revised 19 May 2016; accepted 20 May 2016; published 26 May 2016

34. W. Rozmus and V. T. Tikhonchuk, "Heating of solid targets by subpicosecond laser pulses," Phys. Rev. A **46**(12), 7810–7814 (1992).
35. B. Luther-Davies, E. G. Gamaliĭ, Y. Wang, A. V. Rode, and V. T. Tikhonchuk, "Matter in ultrastrong laser fields," Sov. J. Quantum Electron. **22**(4), 289–325 (1992).
36. M. N. Rosenbluth, "Parametric instabilities in inhomogeneous media," Phys. Rev. Lett. **29**(9), 565–567 (1972).
37. J. L. Kline, D. S. Montgomery, L. Yin, D. F. DuBois, B. J. Albright, B. Bezzerides, J. A. Cobble, E. S. Dodd, D. F. DuBois, J. C. Fernández, R. P. Johnson, J. M. Kindel, H. A. Rose, H. X. Vu, and W. Daughton, "Different $k\lambda_D$ regimes for nonlinear effects on Langmuir waves," Phys. Plasmas **13**(5), 055906 (2006).
38. J. Dawson and C. Oberman, "High-frequency conductivity and the emission and absorption coefficients of a fully ionized plasma," Phys. Fluids **5**(5), 517–524 (1962).
39. T. W. Johnston and J. M. Dawson, "Correct values for high-frequency power absorption by inverse bremsstrahlung in plasmas," Phys. Fluids **16**(5), 722 (1973).
40. S. B. Liu, P. Q. Luo, Y. H. Zhang, S. P. Zhu, and W. Y. Zhang, "Three-dimensional optical trajectory tracing and energy deposition of a laser beam in a laser-driven fusion," Phys. Rev. E **63**(3), 036703 (2001).
41. B. N. Chichkov, C. Momma, S. Nolte, and F. von Alvensleben, A. Tünnermann, "Femtosecond, picosecond and nanosecond laser ablation of solids," Appl. Phys. A **63**, 109–115 (1996).
42. C. Kittel, *Introduction to Solid State Physics*, 5th ed (Wiley, 1976).
43. J. P. Christiansen, D. E. T. F. Ashby, and K. V. Roberts, "MEDUSA a one-dimensional laser fusion code," Comput. Phys. Commun. **7**, 271–287 (1974).
44. A. Djaoui and S. J. Rose, "Calculation of the time-dependent excitation and ionization in a laser-produced plasma," J. Phys. B: Al. Mol. Opt. Phys. **25**, 2745–2762 (1992).
45. E. G. Gamaly, "The interaction of ultrashort, powerful laser pulses with a solid target: Ion expansion and acceleration with time-dependent ambipolar field," Phys. Fluids B **5**(3), 944–949 (1993).
46. H. Cederquist, S. Mannervik, M. Kisielinski, P. Forsberg, I. Martinson, L. J. Curtis, and P. S. Ramanujam, "Lifetimes of some excited levels in Cu I and Cu II," Phys. Scr. **T8**, 104–106 (1984).

1. Introduction

Periodic micro/nanoscale ripple structures generated inside/on any solid surface by means of femtosecond laser (fs-laser) pulses have been attracting a wide spectrum of scientists owing to its extensive applications in nano-optics, fabrication of electronic device, material physics, chemical surface engineering etc. In morphology, when solid surface is irradiated with fs-laser pulse in air/vacuum, ripples are self-formed with an orientation perpendicular to the polarization of the employed laser and with a structuring spatial period (SSP) $\Lambda < \lambda_0$, or even $\Lambda < \lambda_0/2$ [1–3]. This periodic structure in subwavelength scale unfolds renewed interest that it not merely allows the structured or characterized periods on the nanometre scale, but also has enabled us to control the structured patterns to reveal new aspects of their underlying peculiar functions. Thus it is of significant importance to exactly understand the formation process of fs-laser-induced periodic subwavelength structures on solid surface.

As it is well-known, SSP is experimentally proved to be determined by laser parameters (such as energy fluence F_L, wavelength λ_0, pulse duration τ_0, and environment of processing) and material properties. The formation of ripples with SSPs close to or somewhat smaller than λ_0 is universally understood as an interference between the incident fs-laser beam and a surface electromagnetic wave generated at rough surface (so-called surface plasmon polariton) [1–8]. In the case of normal incidence, SSP is usually evaluated by $\Lambda = \lambda_0/n$ [1, 9–11], where n represents the refractive index of the dielectric material. This mode only agrees with experimental results with $\Lambda \sim \lambda_0$ in a narrow fluence regime, however, it fails to interpret the formation of ripples much shorter than laser wavelength. In addition, a stimulated Raman scattering (SRS) model was suggested to try explaining the formation of SSP much shorter than laser wavelength by Sakabe et al. [12], by which the observations in the experiments of some metals [13] and semiconductors [14] targets were interpreted. Nevertheless, as mentioned by Okamuro et al. [13], the SRS process whereby generation of the surface-plasma wave how to result in the formation of periodic structures is not yet fully understood. Other possible mechanisms have been proposed and discussed by taking into account few more inferences, including self-organization [15, 16], second-harmonic generation [2, 3, 7], and interaction

#255940 Received 18 Dec 2015; revised 19 May 2016; accepted 20 May 2016; published 26 May 2016

between laser pulses and surface plasmon polaritons [17–19]. The origin of periodic surface ripple structures with subwavelength scale and its orientation remain a matter of great debate [20, 21], due to extremely intricate interaction of ultrafast laser with solids in the self-formation process, and hence, further investigations are indispensable for this subject.

In Table I, we summarize some experimental results have been reported before, including the ratios of SSP to laser wavelength, along with energy fluences and pulse durations used for different target materials. We also calculate the corresponding laser intensities I_0 by the relation $I_0 = F_L/\tau_0$. One can see that the intensity values aggregate in the range of $5.6\times10^{11}\sim 8.75\times10^{14}$ W/cm^2 which covers the regime of some parametric instabilities and reaches the first ionization threshold for majority of solid materials. According to Keldysh theory [22], the avalanche ionization (by electron impact) and multiphoton ionization will dominate at such intensity values in laser-solid interaction, which consequentially leads to an electron plasma sheet (EPS) formed close to the target surface with underdense density and lower electron temperature determined completely by material properties and laser parameters.

Table 1. **Partial data for periodic surface structures reported on some solid targets [21]: ratios of SSP to wavelength (Λ/λ_0), energy fluences [J/cm^2], pulse durations [fs], and corresponding laser intensity [W/cm^2] values.**

Targets	Λ/λ_0	F_L	τ_0	References	$I_0[\times10^{12}]$
Ti	0.88	0.25	100	[23]	2.5
	0.66	0.067-0.084	65	[24]	1.03-1.29
	0.625-0.88	0.09-0.45	160	[13]	0.56-2.8
	0.645-0.847	0.13	30	[20]	4.3
	0.68	0.5	500	[25]	1.0
Cu	0.5-0.847	0.15-2.0	70, 100	[12]	2.14-2.8
	0.338	0.04-0.1	70, 100	[12]	0.57-1.43
Al	0.675	0.05	65	[26]	0.77
Ni	0.75	0.12	50	[27]	2.4
W	0.775-0.88	0.2-1.1	160	[13]	1.25-6.875
	0.5-0.75	2.5-7.0	33	[28]	75-212
Mo	0.775-0.88	0.2-1.1	160	[13]	1.25-6.875
Au	0.72	0.16	65	[29]	2.46
Pt	0.75-0.88	0.18-0.44	160	[13]	1.125-2.75
	0.69-0.775	0.16	65	[29]	2.46
SS301L	0.81	0.16	90	[30]	1.78
AISI316L	0.625	0.08-0.2	130	[31]	0.615-1.53
	0.69	2.04	150	[32]	13.6
	0.826	0.2-2.0	50	[27]	4.0-40.0

In this paper, we investigate the underlying mechanism for the self-formation of periodic subwavelength surface topological structures on solid surface induced by fs-laser pulses. We propose that STPR driven by fs-laser in EPS gives birth to periodic subwavelength ripple structures (PSRS). Specifically, under the instantaneous strong electrostatic field due to the separation of positive and negative charges, peaks of overdense electrons formed by resonant plasmon wave pull bound ions out solid surface (i.e., ablating process). Thus the resonant plasmon wave pattern on subwavelength scale is "carved" on the surface of target material. On the basis of the STPR model, we have derived analytical formulas which agree with the present and previous observations in structuring experiments.

#255940 Received 18 Dec 2015; revised 19 May 2016; accepted 20 May 2016; published 26 May 2016

2. Surface two-plasmon resonance

When the surface of a solid target is normally exposed to a moderate intensity and linearly polarized fs-laser, the electromagnetic field of incident light that penetrates into the target can be treated as a solution of Maxwell Eqs. coupled to the material Eqs., and the interaction of laser-material falls into the scope of the well-known skin-effect [33–35]. The electrons in the skin layer $d_s = c/\omega_0\kappa$ are heated and ionized by the laser field of leading edge of the incident pulse, where κ is the imaginary part of the refractive index in the Drude approximation and ω_0 is the laser frequency. Almost simultaneously, part of the ionized electrons would brim over the surface and form an EPS with subcritical density near the target-surface with density scale-length $L_z = |n_e/(dn_e/dz)|$, where n_e is the number density of electrons in EPS and z-axis is the propagating direction. In the subsequent interaction driven by the rest pulse, the oscillation of free electrons under the laser electric field $\mathbf{E}_0$ generates two electron plasma waves (Langmuir wave) in opposite directions due to the inversion of the laser electric field, which is shown in Fig. 1(a). Let the target-surface locate in x-y plan $\mathbf{r}_\perp$, then the density fluctuation of electrons associated with Langmuir wave (L-wave) due to the oscillation driven by the laser field can be concisely written as

$$\begin{aligned} n_e'(\mathbf{r}_\perp, z, t) &= n_e(\mathbf{r}_\perp + \mathbf{r}_{os}, z, t) - n_e(\mathbf{r}_\perp, z, t) \\ &\simeq \mathbf{r}_{os}(\mathbf{r}_\perp, t) \cdot \nabla n_e(\mathbf{r}_\perp, z, t) \,, \end{aligned} \tag{1}$$

where $\nabla = \partial/\partial\mathbf{r}$ is a gradient operator and $\mathbf{r} = (\mathbf{r}_\perp, z)$, $\mathbf{r}_{os} = e\mathbf{E}_0(\mathbf{r}_\perp, t)/(m_e\omega_0^2)$ is the spatial amplitude of the electron oscillation in the laser electric field $\mathbf{E}_0(\mathbf{r}_\perp, t)$. Clearly from Eq. (1),

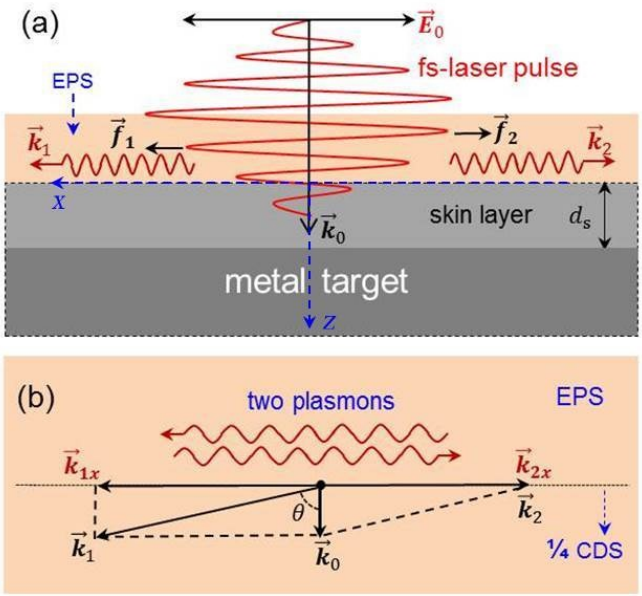

Fig. 1. Schematic process of STPR driven by fs-laser pulse. (a) Generation of two daughter plasmon waves in EPS. (b) Wave vectors of the two plasmon resonances with matching conditions: $k_{1x} = -k_{2x}$ and $k_{1y} = k_0$. CDS denotes critical density surface.

the maximum fluctuation of the electron density (amplitude of L-wave) achieves at its gradient direction (wave vector $\mathbf{k}$), i.e. parallel to laser electric field $\mathbf{E}_0$. Generally, when three waves encounter in the inhomogeneous plasma arousing parametric instabilities may be driven [36]

#255940 Received 18 Dec 2015; revised 19 May 2016; accepted 20 May 2016; published 26 May 2016

as long as the phase relation of the three waves is matched, i.e.

$$\omega_0 = \omega_1 + \omega_2 \quad \text{and} \quad \mathbf{k}_0 = \mathbf{k}_1 + \mathbf{k}_2\,, \tag{2}$$

where $(\omega_0, \mathbf{k}_0)$ is the pump light wave while $(\omega_{1,2}, \mathbf{k}_{1,2})$ may be scattered light waves or plasma waves, or one scattered light wave plus one plasma wave. However, a direct instability process preferentially driven by laser electric field is that: a laser light wave resonantly decays into two L-waves, i.e., a photon $\rightarrow$ a plasmon + a plasmon. Since ω_1 and ω_2 are approximately ω_{pe}, the scattered daughter L-wave has $\omega_1 + \omega_2 \simeq 2\omega_{pe} = \omega_0$ ($\omega_{pe} \simeq \omega_0/2$), suggesting that a resonant two-plasmon decay process occurs at the neighborhood of the quarter-critical density surface ($n_c/4$, where $n_c = m_e/4\pi e^2\omega_0^2 \simeq 3\times10^{-10}\omega_0^2$ is the critical density). The corresponding dispersion relations for the three waves are then

$$\omega_0^2 = \omega_{pe}^2 + c^2k_0^2 \qquad \text{for incident light wave} \tag{3}$$

$$\omega_{1,2}^2 = \omega_{pe}^2 + 3v_e^2k_{1,2}^2 \qquad \text{for plasmon waves,} \tag{4}$$

respectively, where $\omega_{pe} = \sqrt{4\pi e^2 n_e/m_e}$ is the frequency of electron plasma and v_e is the thermal velocity of electrons.

Assuming that a small perturbation of electron density gradient near the $n_c/4$ surface leads one plasmon wave vector (such as $\mathbf{k}_1$) to deviate from the direction of laser electric field or target-planar $\mathbf{r}_\perp$ [see Fig. 1(b)], then the change of $\mathbf{k}_1$ would give rise to a small frequency shift, $(\omega_0/2 - \omega_{pe}) = \pm\delta'$ and $|\delta'| \ll \omega_0/2$. In this case by using matching and dispersion relations, we gain

$$\begin{aligned}\omega_0^2 = (\omega_1+\omega_2)^2 &= \omega_0^2/2 + 3v_e^2(k_1^2+k_2^2) - 2\omega_0\delta' \\ &+ \frac{1}{2}\sqrt{\omega_0^2+12v_e^2k_1^2-4\omega_0\delta'}\cdot\sqrt{\omega_0^2+12v_e^2k_2^2-4\omega_0\delta'}\,.\end{aligned} \tag{5}$$

Expanding Eq. (5) and after daedal mathematical operation, the frequency difference of these two plasmon waves is obtained as

$$\omega_1 - \omega_2 = 3\omega_0\frac{v_e^2}{c^2}\frac{(k_1^2 - k_2^2)}{k_0^2} \tag{6}$$

and $k_{1x} = -k_{2x} = -k_2$ [see Fig. 1(b)]. One can find that, a small difference of $|\mathbf{k}_1|$ and $|\mathbf{k}_2|$ would result in a small frequency shift $(\omega_0/2 - \omega_{1,2}) = \pm\delta$ where "+" means up-shift of the frequency and "−" means down-shift of the frequency and $|\delta| \ll \omega_0/2$. Considering a small angle deviation of $\mathbf{k}_1$ from target surface (i.e., $\theta \approx \pi/2$) due to the density fluctuation as shown in Fig. 1(b), then the dispersion relation of plasmon $(\omega_1, \mathbf{k}_1)$ becomes

$$(\omega_0 - \omega_1)^2 = \omega_{pe}^2 + 3v_e^2\,(\mathbf{k}_0 - \mathbf{k}_1)^2. \tag{7}$$

For convenience in writing, we omit the subscript "1" of ω_1 and k_1 hereinafter and thus have $(\omega_0 - \omega)^2 \simeq \omega_0^2/4 + \omega_0\delta$ and $3v_e^2(\mathbf{k}_0 - \mathbf{k})^2 \simeq \omega_0^2/4 - \omega_{pe}^2 + \omega_0\delta$, in terms of which the wavenumber of surface plasmon can be derived as

$$k = \pm k_0\sqrt{1 + \frac{4}{9}\frac{c^2}{v_e^2}\frac{\delta}{\omega_0}}\,, \tag{8}$$

where the sign $\pm$ means the daughter plasmon waves propagate along opposite directions. Herein one can see that density perturbation is the essential condition for the three-wave

#255940 Received 18 Dec 2015; revised 19 May 2016; accepted 20 May 2016; published 26 May 2016

coupling, as such the three waves can seek the phase matching state by self-organization in the coupling process and finally achieve phase-locked three-wave resonance. Once the phase-locked resonance is created, even if the incident laser pulse has ended, the wave model of STPR would keep oscillating with damping-amplitude way for a period of time just as a pendulum motion suddenly without external force. However in practice, the small perturbation of electron density or frequency is inevitable due to the unpredictable changes of the parameter conditions in the interaction of laser-targets, which undoubtedly results in nonzero density and frequency detunings ($\delta', \delta \neq 0$) in the three-wave coupling. Consequently, this STPR is easily to be driven only if the intensity of pumping laser light reaches threshold condition of the parametric instability growth. In view of this, considering the case of $\omega > \omega_{pe}$ (i.e., $\delta > 0$ situation), we have

$$\delta = \omega - \frac{\omega_0}{2} = \left[\sqrt{4(1+3k^2\lambda_D^2)/5} - 1\right]\frac{\omega_0}{2} = \mu\frac{\omega_0}{2}\,, \tag{9}$$

where $\lambda_D = v_e/\omega_{pe}$ is Debye length and characterizes the spatial characteristic scale. It has been demonstrated that the Langmuir decay instability associated with multiple L-waves generation is driven in the wave-wave nonlinear regime of $k\lambda_D < 0.29$ [37]. Congruously, the change of kinetic parameter is caught in a very narrow range of $0.2886 < k\lambda_D < 0.29$ for STPR and thus we take the frequency shift factor $\mu = 5 \times 10^{-5}$ on an average.

By linearizing Eq. (5), the dispersion relation for three-wave interaction near the location of 1/4 critical density of plasma due to the change of electron temperature is simplified as

$$\frac{\omega}{\omega_0} = \pm\frac{1}{2}\frac{k}{k_0}\left[1 + \frac{2}{9}\left(\mu m_e c^2\right)/T_e\right]^{-1/2}\,, \tag{10}$$

and corresponding $\omega - k$ curve is shown in Fig. 2. Consequently, according to Eqs. (8) and (9) the wavelength of STPR (using $\lambda/\lambda_0 = k_0/k$) writes

$$\lambda = \frac{\lambda_0}{\sqrt{1 + 1.1 \times 10^{-5} m_e c^2/T_e}}\,, \tag{11}$$

where T_e is the temperature of electrons in EPS and $v_e = \sqrt{T_e/m_e}$. In fs-laser-produced plasmas, the electron temperature is mainly proportional to the applied laser intensity (or fluence) and is dependent on the absorption mechanism in the interaction.

3. Estimate of electron temperature

Through Eq. (11), the wavelength of STPR is determined by not only the laser wavelength λ_0 but also the electron temperature T_e which depends on the parameters of light and target material. For the interaction of laser with solid targets, the pulse duration of sub-picosecond appears to be shorter than all characteristic relaxations, such as energy transfer from electrons to ions and electron heat conduction. The major process for laser-target coupling is the electron heating by the laser field, and the interaction falls in the scope of the skin effect. In the meanwhile, the portion of ionized free electrons that overbrim the target surface oscillate in the laser electric field and simultaneously are damped in the electrostatic field formed by target-ions (random inelastic scattering between electron-ion). Therefore these underdense electrons have to be randomly heated instantaneously before the Coulomb ablation occurs. A significant coupling mechanism for laser-plasma interaction in underdense region ($n_e < n_{cr}$) is inverse Bremsstrahlung or collisional absorption [38–40], leading to a conversion from laser into random thermal energy via the absorption of electronic kinetic energy. Thus the temperature

#255940 Received 18 Dec 2015; revised 19 May 2016; accepted 20 May 2016; published 26 May 2016

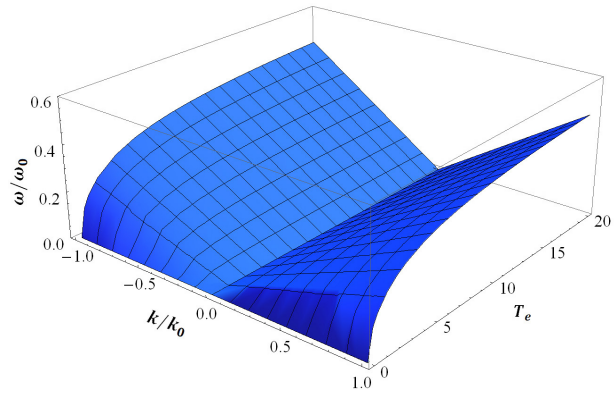

Fig. 2. The dispersion curve near the location of 1/4 critical density of plasma due to the change of electron temperature, where $\mu = 5 \times 10^{-5}$.

of electrons in EPS, in general, is higher than that in the skin layer during the interaction of laser-targets. Whereas for a moderate intensity of incident fs-laser, the scale length of EPS is much smaller than the laser wavelength in such an ultrafast interaction process, and thereby we can substitute the surface electron temperature in skin layer for that in EPS approximatively. According to energy conservation, the Eq. for the electron temperature $T_e(z,t)$ due to the absorption in the skin layer presents [33, 34, 41]

$$C_e n_{e0} \frac{\partial T_e}{\partial t} = \alpha A I_0 \exp(-\alpha z) \,, \tag{12}$$

where $\alpha = 2/d_s$, C_e is the heat capacity (per unit volume) of electrons, A is the absorption coefficient and $A/d_s = 2\omega_0/c$ [33, 34], and n_{e0} is the electron density in the skin layer for metal materials and can be substituted by atom density n_a for nonmetal materials. Due to the

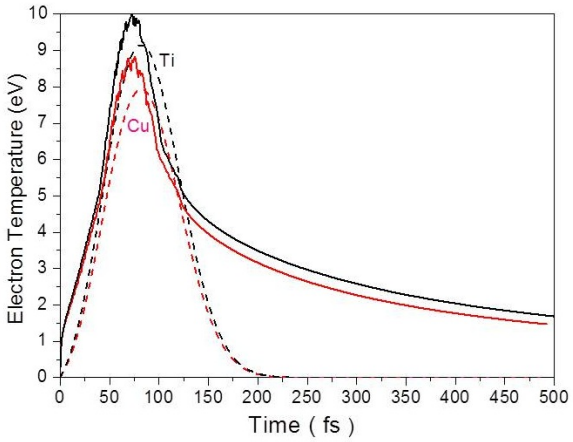

Fig. 3. Transient electron temperatures calculated for Ti (black lines) and Cu (red lines) targets, using the present theory (dashed lines) and the Med103 code (solid lines).

fact that the skin layer is usually much thinner than the heated plasma region, we treat the laser energy absorption in the skin layer as a surface effect. Furthermore, the electron heat capacity

#255940 Received 18 Dec 2015; revised 19 May 2016; accepted 20 May 2016; published 26 May 2016

increases with the increasing of electron temperature from a low temperature degenerate state $C_e = \frac{1}{2}\pi^2 T_e/\varepsilon_F$ up to a maximum value of $C_e \sim 3/2$ for a conventional ideal gas [42], where ε_F is the Fermi energy of electrons. Based on this physical argument we allow the same heat capacity as for an ideal gas because the ionization process has been fulfilled early in the laser pulse, and the electrons are in conditions close to that of an ideal gas. Consequently, the concise linear scaling relation for the electron temperature with respect to fluence at the surface of skin layer irradiated by laser pulses, according to Eq. (12), is obtained as

$$T_e(z=0, t=\tau_0) \simeq 10^{24} \times F_L/(\lambda_0 n_{e0}) \,, \tag{13}$$

where the units of T_e is in eV, F_L in J/cm^2, λ_0 in μm, and n_{e0} in cm^{-3}, respectively.

In order to check the validity of the prediction, the hydrodynamic simulation for a Gaussian pulse incident to metal targets is performed by a one-dimensional Lagrangian code MEDUSA (Med103) [43, 44]. The transient electron temperatures for Cu and Ti are obtained by the simulations with laser intensity of 10^{12} W/cm^2 and wavelength of 0.8 μm, as shown in Fig. 3. One can see that the maximum temperatures obtained from the present prediction are lower than these from the hydrodynamic simulation and also emerge at later moments for both targets. As for these differences, a straightforward reason is that, as mentioned above, Eq. (12) is based on heat diffusion mechanism in materials, and the defined temperature is limited in the skin layer, while the Med103 code is based on inverse Bremsstrahlung absorption mechanism in which the electro-ion scattering effect is taken into account in the heating process.

4. Ablation by STPR wave mode

Although the matching conditions in Eq. (2) allow a broad wave-number spectrum of plasmon waves, the wave mode with $\mathbf{k} \parallel \mathbf{E}_0$ would be preferentially developed, as shown in Eq. (1). We further examine the growth rate of two-plasmon decay process when three-wave-resonance takes place, i.e. [36]

$$\gamma = \frac{\mathbf{k}\cdot\mathbf{v}_{os}}{4}\left[\frac{(\mathbf{k}-\mathbf{k}_0)^2 - k^2}{k|\mathbf{k}-\mathbf{k}_0|}\right] , \tag{14}$$

where $\mathbf{v}_{os} = e\mathbf{E}_0/(m_e\omega_0)$ is the quiver velocity of electron in laser field and $\mathbf{k}$ marks both $\mathbf{k}_1$ and also $\mathbf{k}_2$ for convenience. It indicates that, only when $\gamma > 0$ is satisfied the two-plasmon decay process can develop resonantly and the amplitude of plasmon wave grows steadily. Obviously from Eq. (14) and phase matching relations, the condition of $\gamma > 0$ requires $k < \frac{1}{2}k_0/\cos\theta$. Then the plasmon mode with wave vector approximatively paralleling to the target-planar (large θ angles) has a vector $k \gg k_0$, giving rise to a maximum growth rate $\gamma_m = k_0 v_{os}/4 \simeq 6.25 \times 10^{-4}\sqrt{I_0}$, where I_0 is the amplitude of the laser intensity (in W/cm^2). It shows that a lower intensity threshold of pumping laser is allowed for driving such a parametric resonance of the surface two-plasmon near $n_c/4$. The growing amplitude of the plasmon wave means the increased charge density of the electronegative center in EPS, $\rho = -en'_e$, resulting in a charge separation as shown in Fig. 4. Consequently, a periodic interface electrostatic field is effectively formed on the gradient of the electron density along the normal to the target surface (assuming one dimensional expansion), associating with the amplitude of plasmon wave in EPS. On the basis of such a charge separation, the electrostatic field intensity can be expressed as [45]

$$E_z(x) = -\frac{\varepsilon_{ek}}{e}\cdot\frac{\partial(\ln n_e)}{\partial z} \simeq \frac{F_L}{e d_s n_e \lambda_D} \,, \tag{15}$$

where $\varepsilon_{ek} = m_e v_{e0}^2/2\,(= \varepsilon_{abs} - \varepsilon_w)$ is the kinetic energy of the energetic electrons, v_{e0} is the velocity of electrons rushing out the target surface during the ionization process, ε_{abs} is the

#255940 Received 18 Dec 2015; revised 19 May 2016; accepted 20 May 2016; published 26 May 2016

total energy absorbed by electrons from laser pulse, ε_w is the work function, and λ_D is the Debye length. Thus, once the excitation energy of this electrostatic field force at the peaks of electronegative centers to the target-ion, $eE_z(x_i)\lambda_D$, exceeds its binding energy in the lattice, the target-ions at x_i would be pulled out the target surface by Coulomb ablation (also known as Coulomb explosion or phase explosion) as shown in the schematic diagram in Fig. 4. Consequently, analogous to traditional carving arts by removal material, the wave pattern of STPR is "carved" on the target surface by this Coulomb ablation mechanism. The SSP of the structured ripples is equivalent to the wavelength of STPR ($\Lambda = |x_{i+1} - x_i| = \lambda$) and the scaling Eq., according to Eqs. (11) and (13), is obtained as

$$\Lambda = \frac{\lambda_0}{\sqrt{1+5.62/T_e}}, \tag{16}$$

where the unit of T_e is in eV. It shows that the SSP depends mainly on the laser wavelength and the properties of target materials (temperature dependence). Here one can see that the SSP is explicitly in the subwavelength regime unless an extremely high laser fluence or electron temperature is used. It needs to indicate that the scaling Eq. (16) is also appropriate for dielectric targets, for which the electron temperature T_e should be replaced by dependence relation of laser-dielectric materials. Furthermore, in terms of Eqs. (1) and (5) we also can easily conclude $\mathbf{k} \parallel \mathbf{E}_0$ which means that the orientation of ripples is perpendicular to the polarization of incident laser pulses.

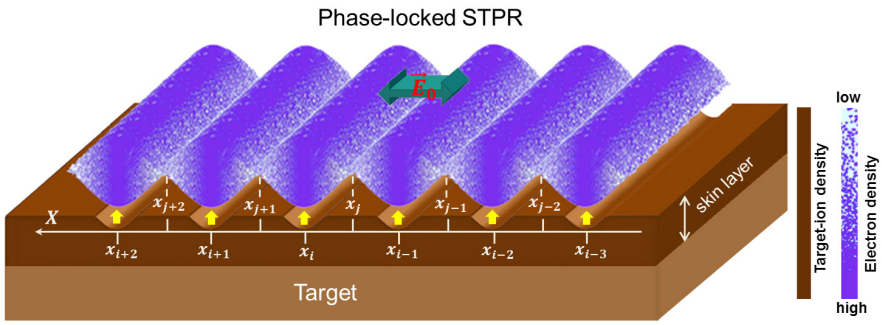

Fig. 4. Schematic mechanism of phase-locked STPR wave producing periodic Coulomb ablation. The coordinates ..., x_{i-1}, x_i, x_{i+1}, ... label the positions of electronegative centers formed by the peaks of wave electrons due to the STPR, and the skin-layer denotes the electropositive surface produced by the bound target-ions. Coulomb ablation occurs only at the peaks of overdense wave electrons due to the electrostatic field between electronegative centers and electropositive surface of target.

In order to assess the time necessary to fulfill the Coulomb ablation (i.e., Coulomb explosion), we define the Debye length as a basic distance over which the target ion is considered to be dragged out of the lattice. Therefore, the energy condition for Coulomb ablation accords with $m_i v_{i0}^2/2 = eE_z(x_i)\lambda_D - (\varepsilon_b + \varepsilon_w) > 0$ and the change of ion momentum meets Newton's law $m_i \mathrm{d}v_{i0}/\mathrm{d}t = eE_z(x_i)$, where ε_b is the binding energy of ions in the lattice and v_{i0} is the initial velocity of ions out of the lattice. Consequently, the time necessary to accelerate and ablate an ion can be roughly evaluated by the relation of

$$t_{acc} = \lambda_D / v_{i0} = \omega_{pe}^{-1} \frac{v_{e0}}{v_{i0}}. \tag{17}$$

#255940 Received 18 Dec 2015; revised 19 May 2016; accepted 20 May 2016; published 26 May 2016

As an example to conservatively estimate the acceleration time of an ion in copper target ($\varepsilon_w =$ 4.65 eV and $\varepsilon_b = 3.125$ eV [42]) at wave peaks $x_{i\pm\cdots}$, we consider that the electron density at $x_{i\pm\cdots}$ (wave peaks of STPR mode) is ten times the critical density and the absorbed energy ε_{abs} is approximatively replaced by electron Fermi temperature (≈ 7.0 eV), consequently, this time gives less than 40 fs at $F_L = 0.5\,\mathrm{J/cm^2}$ and $\lambda_0 = 0.8\,\mu$m ($d_s \approx 67$ nm). In this case, it indicates that the Coulomb ablation is possibly achieved as long as the lifetime of STPR state remains over 40 fs.

It needs to emphasize that the periodicity of surface structures with wave pattern will disappear (taking on crater shape) if the electrostatic field forces at STPR valleys $x_{j\pm\cdots}$ are so strong so that bound ions can be effectively dragged out of target surfaces. Therefore, the applied laser fluence in structuring experiments is necessarily to be limited below an upper ablation threshold, which will be discussed in another paper.

5. Experimental verification

In order to confirm the present physical model we carried out experimental verification. Our experimental setup is equipped with a commercial fs-laser system (Ti : sapphire Micra 10 and regenerative amplifier Legend Elite-USP-HE, Coherent Corp.) with 60 fs pulse duration, 800 nm central wavelength, 3.5 mJ/pulse, and repetitive rate of 1 kHz. The pulse laser beam was shaped into a nearly flat-top profile in energy distribution by a commercial beam shaping system (Focal-π Shaper 9, AdlOptica Corp.). The shaped incident beam was focused normally onto the target surface by a lens with 100 mm focal length and its profile at focal position shows a circular shape with diameter of $\sim 60\ \mu$m. The laser fluence was varied in the range of $0.05 \sim 2.0\,\mathrm{J/cm^2}$ in our experiments. To implement time-resolved spectroscopy measurements from fs-laser structuring, we used an ICCD camera (PI Corp., USA) with a basic gate width (i.e.exposure time for one triggering) of $\tau_\Delta = 2$ ns.

5.1. *Lifetime of surface plasmon induced by fs-laser*

As mentioned above, the lifetime of the surface plasma state produced in the interaction of laser-targets should be long enough in order to realize the periodic Coulomb ablation by the phase-locked STPR. We know that laser-produced plasma (charged particles) states would emit abundant electromagnetic radiations continuously (continuous spectrum, CS) due to their random motions, and while the electrons begin to recombine with their parent ions the

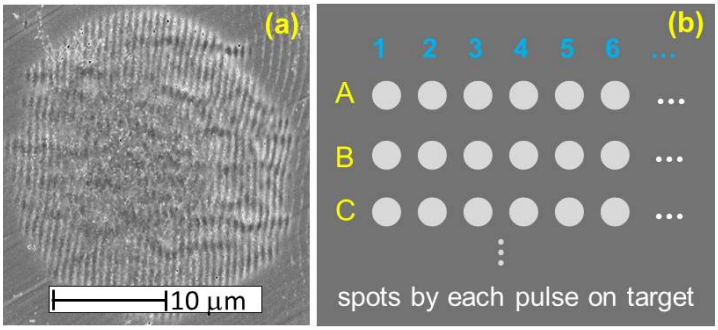

Fig. 5. Schematic illustration of spot matrix for the measurement of time-resolved spectra. (a) SEM image taken on Cu target in fs-laser structuring experiment. (b) Spot matrix for time-resolved spectra on target shown in (a). Spots with different shutter/trigger time are grouped in A, B, C etc.

#255940 Received 18 Dec 2015; revised 19 May 2016; accepted 20 May 2016; published 26 May 2016

characteristic line spectra (CLS) radiate because of the state transition between energy levels in atoms. Therefore, the duration δt_p from the emission of CS to the appearance of the first CLS characterizes a pure plasmon state. In other words, the total number of free electrons remains unchanged during the time from the end of laser pulses to the emission of the first CLS. Here we define δt_p as the lifetime of surface plasmon, which is the basis for the existence of plasmon wave (as well as the STPR). In view of this feature, to evaluate the duration δt_p, we have performed a series of time-resolved spectroscopy measurements. The camera shutter is triggered by the trigger signal output from the fs-laser system, and the emitted spectra are guided into a spectrometer through a grating and detected by an ICCD camera.

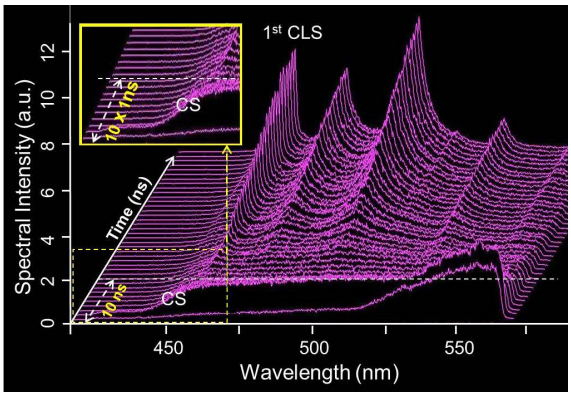

Fig. 6. Time-resolved spectra measured on Cu target by irradiation with linearly polarized 60 fs laser pulses with a central wavelength of 800 nm and a fluence per pulse of 0.4 J/cm^2.

In order to generate optimized periodic surface ripple structures, firstly, a linearly polarized fs-laser with a fluence of 0.4 Jcm^{-2}/pulse is applied at a fixed position on Cu-metal surface. After successively irradiated by 100 pulses, the scanning electron microscope (SEM) image is shown in Fig. 5(a). The time evolution of the emitted spectra can be resolved by varying the trigger time continuously. In addition, to minimize the inhomogeneous effect, different spots on the target surface are measured, forming a spot matrix, as shown in Fig. 5(b). Specifically, each group has the same trigger time, and tens of spectra (noted as 1, 2, 3, 4, 5, 6,...) at different spots in the same group are integrated. For example, group "A" contains spectra at trigger time t_1, while the second group "B" is triggered at t_2, then a time interval $\Delta t\,(=t_2-t_1)$ can be obtained. Figure 6 shows the measured time-resolved spectra from Cu target with a time interval of 1 ns. One can find that the first CLS ($5s'^4D_{7/2} \rightarrow 4p'^4F^0_{9/2}$, 465.11 nm) [46] shows up at the 10th spectral curve. Therefore, in terms of time-resolved spectra we can conclude that the lifetime of surface plasmon (electron) approximates 10 ns which is at least five orders of magnitude longer than the acceleration time of target-ions.

5.2. Carving effect of STPR wave patterns

In order to verify the carving effect resulted from STPR mechanism, we carried out structuring experiments by using two beams multi-irradiating W-target statically, as illustrated in Fig. 7(a). The sample surface was only simply polished mechanically to avoid too high reflectivity, and the pulse profile was properly shaped by a Focal-π Shaper 9 system. The average energy of the incident laser can be altered from 1 μJ to 3.5 mJ by using a variable density filter, and the pulse account is controlled by an synchronized electromechanical shutter (not shown in the picture).

To show the carving effect of different wave patterns induced by STPR, a linearly polarized normal incident fs-laser beam is equally split in two beams by a beam splitter, denoted as p-

#255940 Received 18 Dec 2015; revised 19 May 2016; accepted 20 May 2016; published 26 May 2016

① and p-②, with electric field intensities $\mathbf{E}_{01}$ and $\mathbf{E}_{02}$. The delay time between these two beam is tuned by a motorized time-delay-line (TDL) and the polarization direction of p-② ($\mathbf{E}_{02}$) can be altered by a half wave plate ($\lambda/2$). In this two-beam structuring experiment the delay time $\Delta\tau$ between p-① and p-② was chosen at 100 ns so as to have $\Delta\tau$ much larger than the relaxation time of electron heat diffusion. The polarization directions of two beams were selected as mutually perpendicular ($\mathbf{E}_{01} \perp \mathbf{E}_{02}$), and the whole structuring process was performed in air. Thus, the observed results positively reveal the effect of alternant ablating of two wave patterns by STPR with $\mathbf{E}_{01} \perp \mathbf{E}_{02}$ (layer-carving effect).

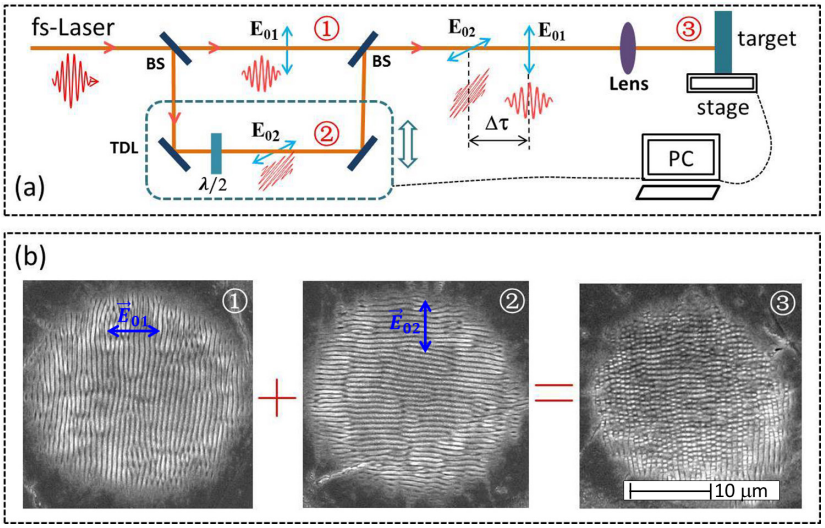

Fig. 7. (a) Overview of the experimental setup for periodic ripple experiments using two beams with perpendicular light polarizations. BS is a non-polarizing 50/50% beam splitter, $\lambda/2$ is a half wave plate, and TDL is a motorized time-delay-line. (b) Ripples (SEM) produced by pulses with horizontal (①), vertical (②), and dual (③) polarizations. All pictures have a 10 μm scale.

Figure 7 (b) shows SEM images under the irradiation of fluence 0.6 J/cm^2, indicating clear layer-carving effects: image ① and image ② are produced by beam p-① (horizontal polarization) and beam p-② (vertical polarization), respectively; while image ③ is a combination produced by p-① and p-②. This demonstrates that the wave patterns for STPR driven by p-① and p-② beams are effectively carved by removal material on the target surface, the orientation of structured ripples is perpendicular to the polarization direction ($\mathbf{E}_0$) of the driving laser, the SSP is located in subwavelength ($\sim 0.75\,\lambda_0$), and especially, the topological feature of layer-carving produced by STPR wave is significantly highlighted here.

5.3. Comparison of observed and predicted SSPs

The self-formation of periodic surface structures by fs-laser pulses is determined by the underlying physical mechanism, with the structure morphology depending on material properties, laser parameters, and processing methods. However, even for the same materials and roughly identical laser fluences, SSP results from different literatures can deviate from each other, as one can see in Table I. These differences may arise from the estimation for the diameter of laser focal spot, selection from their SEM images, processing environment, etc. In order to compare experimental observations with theoretical predictions by Eq. (16), three target materials, Cu, Ti, and W, are selected as the examples in our experiments. A shaped linear

#255940 Received 18 Dec 2015; revised 19 May 2016; accepted 20 May 2016; published 26 May 2016

polarized fs-laser beam with 800 nm wavelength was normally focused on the target surface continuously by 100 pulses, with which the ranges of laser fluence from 0.05 to 1.2 J/cm^2 for Cu target, 0.05 to 1.2 J/cm^2 for Ti target, and 0.2 to 2.0 J/cm^2 for W target were employed, respectively. Figure 8 summarizes our observations and previous some typical experimental data for SSP as a function of laser fluence. In Fig. 8(a), one can see small deviations for different materials in theory.

For Ti target shown in Fig. 8(c), much larger deviations appear between the observations reported in [13, 23, 24] and our prediction, however our calculation agrees very well with the results observed in our experiment and in [25]. We should emphasize that, for Cu target shown in Fig. 8(b), the observed data are in good agreement with the prediction and especially, the present physical model can self-consistently explain the ripple structures with SSPs shorter than half of laser wavelength ($<\lambda_0/2$) at small laser fluences (≤ 0.1 J/cm^2) [12].

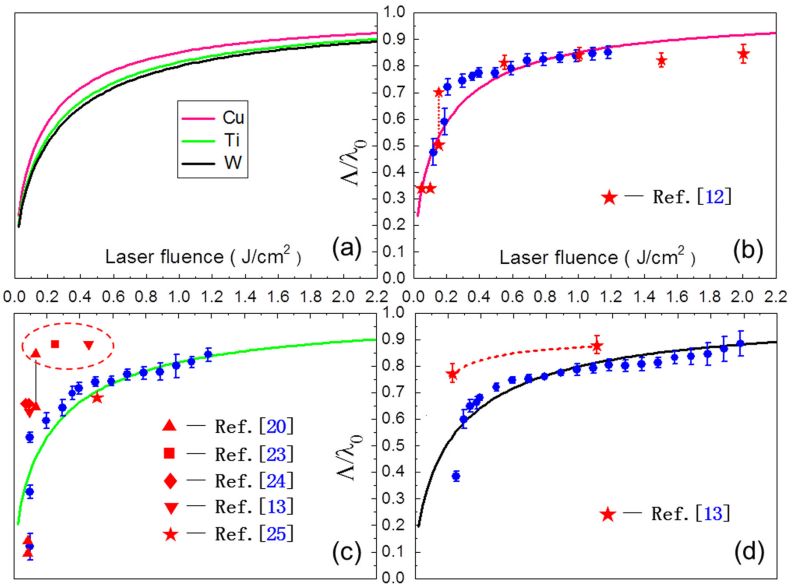

Fig. 8. Ratios of ripple's SSP to laser wavelength (Λ/λ_0) vs laser fluence. (a) Theoretical predictions by Eq. (16) for Cu, Ti, and W targets. (b)-(d) Comparisons of observed (discrete symbols) and prophetic (solid lines) results for Cu, Ti, and W targets. Blue dots are observed results from our experiments.

6. Discussion and conclusion

We propose here a new mechanism for surface structuring on solid surfaces by fs-laser pulses, and present an analogous surface carving notion arising from phase-locked STPR wave pattern. The interaction is characterized by laser intensity in the range of 10^{11} to 10^{14} W/cm^2, with a pulse duration of tens of femtoseconds. We note the interaction time is much shorter than the plasma expansion time, the heat conduction time, the electron-ion energy transfer time, and especially the ion respond time in which the ion can be considered as an immobile electropositive background. Under such conditions the ionization of any target material is practically realized. The electron density perturbation ($\mu \neq 0$) facilitates the phase matching of three-wave resonance in EPS formed by hot electrons escaping from target surfaces. Therefore, L-wave ablation resulted from STPR is responsible for the self-formation of periodic

#255940 Received 18 Dec 2015; revised 19 May 2016; accepted 20 May 2016; published 26 May 2016

subwavelength ripple structures. The notion of L-wave pattern carving (Coulomb ablation) occurs in the acceleration of target-ions at the L-wave peaks located in the periodic interface electrostatic field created between negative electricity centers and target ions. The wavelength of STPR is closely determined by electron temperature, as shown in Eq. (11). In the estimation of electron temperature in EPS, the loss of laser energy in ionization process is ignored and T_e in surface plasmon is replaced by that in the skin layer of solids, which is valid only in the case of low laser intensities ($< 10^{14}$ W/cm^2).

In summary, we derived explicit analytical formulas for dispersion relations between phase-locked STPR, laser wavelength (wavenumber), SSP, and electron temperature in ultrafast interaction between fs-laser and solid surfaces. The relevant dynamics in the present model, including relaxation of surface plasmon, electron heating, and surface Coulomb ablation of L-wave pattern, were verified respectively by time-resolved spectroscopy, numerical simulations, and two-beam structuring experiments. According to the topological features of PSRS generated by time-delay two-beam method we propose a "layer-carving" notion. The theoretical calculations agree with both our and previous experimental data, and especially can self-consistently explain SSP $\Lambda < \lambda_0/2$ at low fluences. Our model can be readily extended to more materials including metals and dielectrics under fs-laser exposure.

Acknowledgments

We gratefully acknowledge support for this work from the National Natural Science Foundation of China (Grant No. 51275012) and NSAF of China (Grant No. U1530153), the Ministry of Science and Technology of China Major Project of Scientific Instruments and Equipment Development (Grant No. 2011YQ030112), and the Beijing Commission of Education (No. KZ201110005001).

#255940 Received 18 Dec 2015; revised 19 May 2016; accepted 20 May 2016; published 26 May 2016